Research Article Vol. 29, No. 13 / 21 June 2021 / Optics Express 20379
Optics EXPRESS

Angular selectivity based on a double-resonance periodic array of scatterers

LIN ZHOU AND ZHONGXIANG SHEN*

School of Electrical and Electronic Engineering, Nanyang Technological University, Singapore 639798, Singapore
*ezxshen@ntu.edu.sg

Abstract: A double-resonance periodic array of scatterers is proposed to achieve angular selectivity in this paper. By properly designing the scatterers' structure and dimensions, bandpass and band-stop resonances are produced by the periodic array at the same frequency under the normal and oblique incidences, respectively, resulting in excellent angular selectivity. The periodic array consists of two identical scatterer layers stacked together with an air spacer. To demonstrate the design concept, a sample of the periodic array with an operating frequency of 10 GHz is designed for the angular selectivity of TE-polarized incident waves. Measurements of the sample are conducted for verification. The simulated and measured results both show good angular selectivity with high transmission under the normal incidence and low transmission under the oblique incidence of large angles.

1. Introduction

Over the past several decades, manipulation and selection of electromagnetic (EM) waves have attracted a lot of attention, with respect to its three fundamental properties: frequency [1–3], polarization [4,5], and propagation direction/angle [6–21]. Among them, angular selectivity [9–21], allowing EM waves of certain angles to transmit, while blocking waves from other angles, has not been extensively investigated though it may play an important role in many applications, such as brightness enhancement and privacy protection in the display industry [9], and minimizing the antenna's side lobes [10,11].

One conventional approach for realizing the angular selectivity is using geometrical optics [12,13]. A reflective broadband angle-selective filter composed of parabolic directors was proposed in [12], where the incident light is funneled through with an incident angle less than 5.6°, while strongly reflected at larger angles.

Another approach is utilizing the Brewster angle principle. A thick metal plate with an array of slits can excite surface plasmon polaritons and provide a Brewster-like broadband extraordinary transmission for the transverse magnetic (TM) incident wave [14,15]. Stacks of one-dimensionally periodic photonic crystals were studied to generate a Brewster angle and provide broadband angular selectivity [16,17]. A bilayer uniaxial dielectric-magnetic slab was proposed to provide polarization-insensitive Brewster angle and critical angle for angular-dependent transmission [18].

Moreover, the angular selectivity can be obtained by using resonant scatterers. Split-ring scatterers and complementary split-ring scatterers were studied for obtaining the angular selectivity in [19–21], where an axial magnetic resonance [22] is excited and manipulated to reflect or transmit the oblique incidence. However, the bandwidth of the magnetic resonance is typically narrow.

In this paper, angular selectivity based on a double-resonance periodic array of scatterers is studied. By properly designing the periodic array, bandpass and band-stop resonances are generated for the angular selectivity with high and low transmission under the normal and oblique incidences, respectively, at the same frequency. The double-resonance design concept is effective

#428005 https://doi.org/10.1364/OE.428005
Journal © 2021 Received 15 Apr 2021; revised 3 Jun 2021; accepted 4 Jun 2021; published 15 Jun 2021

Optics EXPRESS

for both transverse electric (TE) and TM polarizations. A sample of the periodic array with an operating frequency of 10 GHz is designed to demonstrate the angular selectivity of TE-polarized incidences. Good angular selectivity with high transmission under the normal incidence and low transmission under the oblique incidence of large angles is observed in the simulations and measurements.

2. Design concept

Periodic arrays of resonant scatterers are widely employed for realizing special properties, such as frequency and polarization selectivity [1–5], in the microwave and optical regimes. Similarly, the resonant scatterers are also capable of achieving angular selectivity, controlling the transmission or reflection of an incident wave based on its incident angle. For example, the angular selectivity with high transmission under the normal incidence and high reflection or low transmission under the oblique incidence, as illustrated in Fig. 1, can be achieved by exciting a bandpass or band-stop resonance under the normal or oblique incidence. Based on this resonant concept, we propose a double-resonance periodic array of scatterers for the angular selectivity. The periodic array serves as a bandpass resonator under the normal incidence, while it acts as a band-stop resonator at a large incident angle.

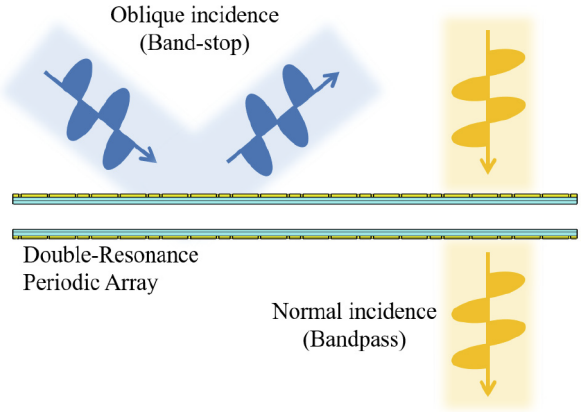

Fig. 1. Illustration of angular selectivity, where transmission and reflection are controlled by the double-resonance periodic array based on incident angles.

It is well known that the reflection-transmission properties of periodic arrays can vary with the incident angle [1]. However, it is very difficult to achieve a very large equivalent reactance and a nearly zero equivalent reactance by a single-layer scatterer structure under the normal and oblique incidences at the same frequency to generate high and low transmission. Therefore, our periodic array is based on a double-layer structure, whose configuration is shown in Fig. 2(a). It comprises two layers of scatterers separated by an air spacer of thickness h_2. Each layer is a printed-circuit-board (PCB) and the PCB laminate used in the design is RT5880 with a relative permittivity of 2.2 and a thickness h_1 of 0.508 mm. Conducting scatterers are printed on the top or bottom layers of the PCBs.

Two respective resonances can be generated by this double-layer structure to control the transmission magnitude of the normal and oblique incidences, resulting in the desired angular selectivity. One resonance is produced by a single layer of scatterers. While another resonance is generated by two layers of scatterers under an incident wave with a different angle. Multiple reflections are excited between the two layers of scatterers, leading to a Fabry-Perot resonance. The equivalent circuit model of the periodic array is constructed to explain the double resonances

Optics EXPRESS

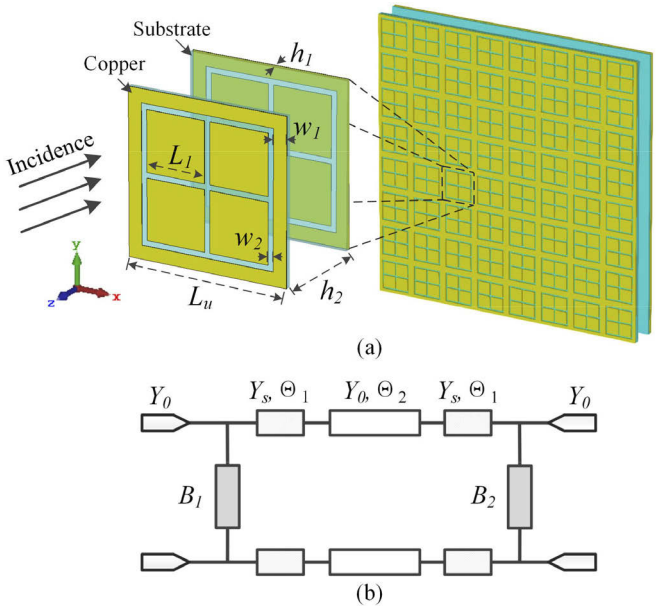

Fig. 2. (a) Structure of the proposed double-resonance periodic array of scatterers and (b) its equivalent circuit model.

and to formulate the design guidelines. The circuit model is derived following the process in [23,24] and shown in Fig. 2(b). The air spacer is modeled as a transmission line section with an admittance of Y_0 and an electrical length of $\Theta_2 = k_0 h_2$. The PCB substrates are represented as transmission line sections with Y_s and Θ_1. The conductive scatterers are represented as two shunt components: susceptance B_1 and susceptance B_2.

In our design, the PCB substrate is very thin and with a low relative permittivity. Therefore, they may be ignored in this circuit-model analysis for simplicity. Then the reflection coefficient of the equivalent circuit model can be expressed as

$$\Gamma = \frac{Y_0 - jB_1 - \frac{Y_0[Y_0+(B_2-jY_0)\cot\Theta_2]}{jB_2+Y_0-jY_0\cot\Theta_2}}{Y_0 + jB_1 + \frac{Y_0[Y_0+(B_2-jY_0)\cot\Theta_2]}{jB_2+Y_0-jY_0\cot\Theta_2}}. \tag{1}$$

All of the above parameters of the equivalent circuit model are variables of the incident angle θ. They can be written as B_1^{TE}, B_2^{TE}, $Y_0^{TE} = Y_0 \cos\theta$, and $\Theta_2^{TE} = \Theta_2 \cos\theta$ for the oblique TE-polarized incidence. On the contrary, they are B_1^{TM}, B_2^{TM}, $Y_0^{\mathrm{TM}} = Y_0/\cos\theta$, and $\Theta_2^{TM} = \Theta_2 \cos\theta$ for the oblique TM-polarized incidence [25].

Due to the cascaded layered structure, a band-stop resonance with $|\Gamma| = 1$ can be achieved for the double-resonance periodic array under the oblique incidence by designing the first or second layer of scatterers with

$$1/B_1^{TE,\theta\neq 0} \text{ or } 1/B_2^{TE,\theta\neq 0} = 0,\ 1/B_1^{\mathrm{TM},\theta\neq 0} \text{ or } 1/B_2^{TM,\theta\neq 0} = 0 \tag{2}$$

for TE and TM polarizations, respectively.

On the other hand, the equivalent susceptances B_1 and B_2 change with different incident angles, and they should be different from 0 under the normal incidence. With properly designed B_1, B_2, and Θ_2, the impedance of the periodic array can be matched to free space under the normal incidence, generating the required bandpass characteristics. Based on (1), the bandpass ($|\Gamma| = 0$)

Optics EXPRESS

condition is obtained, which is given as

$$B_1^{\theta=0} = B_2^{\theta=0} \neq 0\,, \quad \cot\Theta_2 = \frac{B_1^{\theta=0} B_2^{\theta=0}}{Y_0(B_1^{\theta=0} + B_2^{\theta=0})}. \tag{3}$$

Under this condition, a Fabry-Perot resonance with a bandpass response is constructed by the periodic array, resulting in high transmission and low insertion loss [26,27]. Therefore, the angular selectivity is produced through designing the periodic array to satisfy (2) and (3) at the same time.

Based on the above analyses, the design of the double-resonance periodic array can be summarized by the following steps.

1) Design a single-layer scatterer structure with $1/B^{\theta=0} \neq 0$ and $1/B^{\theta\neq0} = 0$ under the normal incidence and oblique incidence of a large angle, respectively. $1/B^{\theta\neq0} = 0$ under the oblique incidence is responsible for the band-stop resonance generating low transmission.

2) Due to the requirement that $B_1^{\theta=0} = B_2^{\theta=0}$, the second layer of scatterers is set to be identical to the first layer of scatterers. Therefore, we only need to determine the distance h_2 between the scatterer layers based on (3), by

$$\cot k_0 h_2 = \frac{B}{2Y_0} \tag{4}$$

to produce the bandpass resonance resulting in high transmission.

The above design procedure is effective for both TE and TM polarizations because Step 1) can be applied to TE and TM polarizations. To further demonstrate the design concept and guidelines, a periodic array with an operating frequency of 10 GHz is designed for achieving the angular selectivity of TE polarization in Section 3.

3. Design example

As discussed in [1], some classical scatterer patterns, such as dipole and Jerusalem cross, can provide a fundamental resonance with a band-stop response, satisfying (2) under the oblique incidence. However, their equivalent susceptance B only slightly changes at the fundamental resonance frequency with different incident angles. $1/B$ under the normal incidence would be very close to 0, which may not be beneficial for realizing a stable bandpass resonance by cascading two layers.

Therefore, a single-layer scatterer with slot patterns is designed, as seen in Fig. 2(a), whose first higher-order resonance is utilized for providing $1/B^{\theta\neq0} = 0$. The dimensions and simulated transmission magnitudes of the single-layer scatterer under the incidences of $\theta = 0°$ and 60° are given in Fig. 3(a). It is observed that the fundamental resonance of the scatterer is a bandpass response with a resonant frequency of 6.9 GHz. The transmission coefficient is very stable with respect to the incident angles at 6.9 GHz. Nevertheless, its first higher-order resonance is a band-stop response, which is sensitive to the incident angle. Band-stop resonances are observed at 10 GHz and 9.2 GHz under the TE- and TM-polarized incidences of $\theta = 60°$, respectively. The simulated transmission magnitudes and equivalent reactances ($-1/B$) of the single-layer scatterer under the TE-polarized incidences of different angles at 10 GHz are shown in Fig. 3(b). The simulated transmission magnitude is less than −15 dB with an incident angle larger than 52°. The equivalent reactance is −4.1 Ω at $\theta = 60°$, which is very close to 0 and satisfies (2). On the other hand, the reactance is distinctly different at $\theta = 0°$, as −177.6 Ω.

Based on the single-layer scatterer, a double-resonance periodic array is formed for the angular selectivity of TE polarization. The distance h_2 between the two layers can be calculated in

Optics EXPRESS

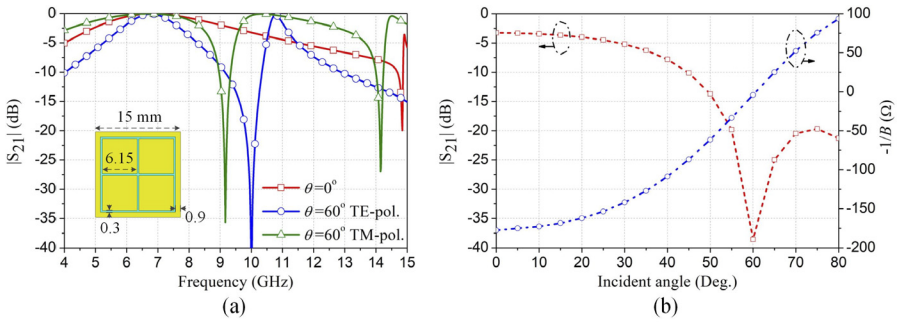

Fig. 3. (a) Simulated transmission magnitudes ($|S_{21}|$) of a single-layer scatterer employing a slot pattern under the incidences of $\theta = 0°$ and 60°, and (b) simulated transmission magnitudes and equivalent reactances ($-1/B$) of the single-layer scatterer under the TE-polarized incidences of various angles at 10 GHz.

accordance with (4), as $h_2 = (0.24+n)\lambda/2$, where $n = 0, 1, 2\ldots$, and λ is the free-space wavelength at 10 GHz. Due to the influence of the PCB substrates, the optimal h_2 may be slightly different from the calculated one. Therefore, full-wave simulations are carried out for further optimizations. The simulated transmission magnitudes of the double-resonance periodic array with $h_2 = 2.5$, 17.5, and 32.5 mm, corresponding to $n = 0$, 1, and 2, under the TE-polarized incidences of $\theta = 0°$ and 60°, are shown in Fig. 4(a). Bandpass resonances are observed with all three distances under the normal incidence of $\theta = 0°$. On the other hand, band-stop resonances are produced under the oblique incidence of $\theta = 60°$ with $h_2 = 17.5$ and 32.5 mm, but the transmission magnitude is still high with $h_2 = 2.5$ mm due to the strong coupling between the two layers. Therefore, a shorter distance $h_2 = 17.5$ mm is selected for our design.

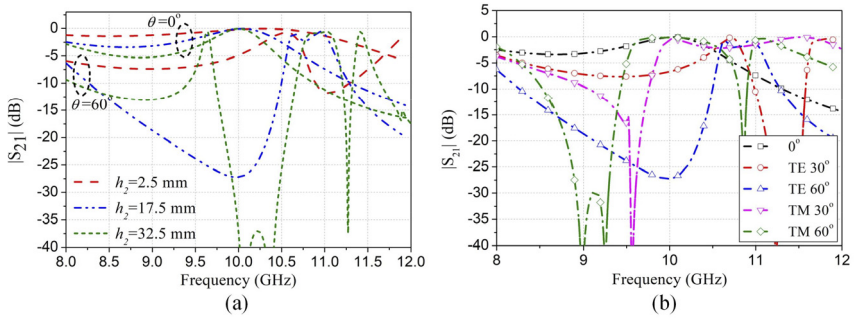

Fig. 4. (a) Simulated transmission magnitudes of the double-resonance periodic array with $h_2 = 2.5$, 17.5, and 32.5 mm under the TE-polarized incidences of $\theta = 0°$ and 60°, and (b) simulated transmission magnitudes of the double-resonance periodic array with $h_2 = 17.5$ mm under the TE- and TM-polarized incidences of $\theta = 0°$, 30°, and 60°.

The simulated transmission magnitudes of the double-resonance periodic array under the TE- and TM-polarized incidences of $\theta = 0°$, 30°, and 60° are shown in Fig. 4(b). The transmission magnitudes under the oblique TM-polarized incidence are still high at 10 GHz, different from those under the oblique TE-polarized incidence. Moreover, the transmission magnitudes of the periodic array under the TE-polarized incidences with various incident angles at 10 GHz are shown in Fig. 5, where good angular selectivity is demonstrated. The transmission magnitude is less than −1 dB with the incident angle smaller than 16°, and it decreases with the increasing incident angle, reaching −20 dB with an incident angle of 48°.

Optics EXPRESS

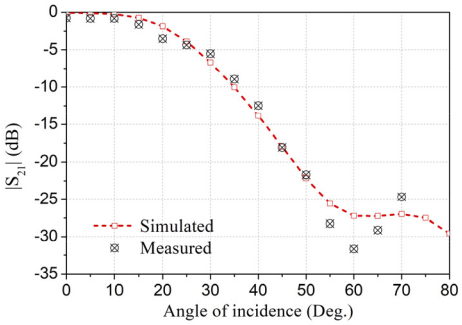

Fig. 5. Transmission magnitudes of the double-resonance periodic array under the TE-polarized incidences of various incident angles at 10 GHz.

The designed double-resonance periodic array is fabricated and measured to verify the design concept and to assess the angular selectivity performance. The fabricated prototype and measurement setup are shown in Fig. 6. The prototype of the periodic array comprises 18 × 18 unit cells with a total size of 270 mm × 270 mm (9λ × 9λ). In the measurement, two horn antennas (LB-20245-SF) are utilized to transmit and receive signals, respectively, and a vector network analyzer (Agilent E8362B) is employed to analyze the signals. Time-domain gating is used in the analyses for eliminating multi-path transmissions. The periodic array is placed in the middle window of a large metallic screen to minimize the effect of edge diffraction. The transmission magnitudes of the periodic array can be achieved by

$$|\mathrm{S}_{21}|_{\mathrm{array}} = \frac{|T_{21}|_{\mathrm{array}}}{|T_{21}|_{\mathrm{air}}} \tag{5}$$

where $|T_{21}|_{\mathrm{air}}$ and $|T_{21}|_{\mathrm{array}}$ are the measured transmission magnitudes between the horn antennas without and with the periodic array, respectively.

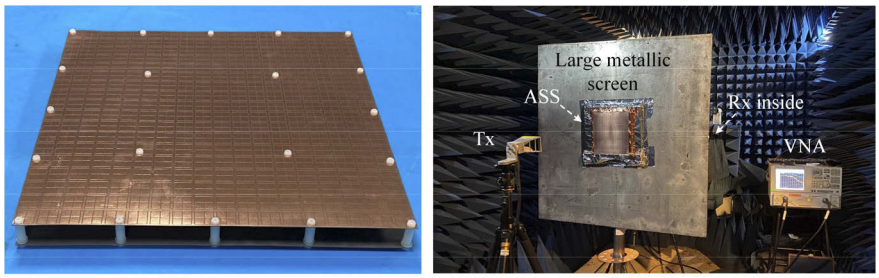

(a) (b)

Fig. 6. (a) Fabricated prototype of the double-resonance periodic array and (b) its measurement setup.

Figure 7 shows the measured transmission magnitudes of the fabricated periodic array under the TE-polarized incidences of $\theta = 0°$, 30°, and 60° at different frequencies. A good agreement between the simulation and measurement is observed. Bandpass and band-stop resonances are detected under the TE-polarized incidences of $\theta = 0°$ and 60°, respectively. Moreover, the transmission magnitudes under the TE-polarized incidences with various incident angles at 10 GHz are measured, as seen in Fig. 5, which agree well with the simulations, verifying the validity of the periodic array design. The measured transmission magnitudes are −0.7 dB and

Optics EXPRESS

−31 dB for $\theta = 0°$ and 60°, respectively, and the transmission magnitude is less than −20 dB with $\theta > 50°$.

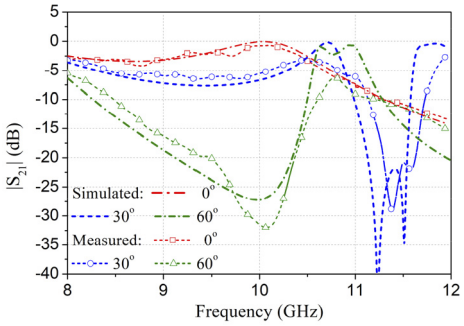

Fig. 7. Transmission magnitudes of the double-resonance periodic array under the TE-polarized incidences of $\theta = 0°$, 30°, and 60°.

4. Conclusion

In summary, a double-resonance periodic array of scatterers has been studied for providing angular selectivity. Bandpass and band-stop resonances have been generated by the properly designed periodic array under the normal incidence and oblique incidence of a large angle, respectively, resultantly producing the excellent angular selectivity. A double-resonance periodic array with TE-polarized angular selectivity has been designed to demonstrate the design concept and guidelines in the microwave regime. Measurements of the periodic array have been conducted, where a good agreement between simulation and measurement is observed. Good angular selectivity with high transmission under the normal incidence and high rejection under the oblique incidence has been successfully demonstrated.

Disclosures. The authors declare no conflicts of interest.

Data availability. Data underlying the results presented in this paper can be obtained from the authors upon reasonable request.

References

1. B. A. Munk, *Frequency Selective Surfaces: Theory and Design* (John Wiley & Sons, 2000), Chap. 2.
2. Y. Shang, Z. Shen, and S. Xiao, "On the design of single-layer circuit analog absorber using double-square-loop array," IEEE Trans. Antennas Propag. **61**(12), 6022–6029 (2013).
3. Z. Zhu, Y. Li, J. Zhang, J. Wang, W. Wan, L. Zheng, M. Feng, H. Chen, and S. Qu, "Absorptive frequency selective surface with two alternately switchable transmission/reflection bands," Opt. Express **29**(3), 4219–4229 (2021).
4. H. F. Ma, G. Wang, G. S. Kong, and T. J. Cui, "Broadband circular and linear polarization conversions realized by thin birefringent reflective metasurfaces," Opt. Mater. Express **4**(8), 1717–1724 (2014).
5. F. Zeng, L. Ye, L. Li, Z. Wang, W. Zhao, and Y. Zhang, "Tunable mid-infrared dual-band and broadband cross-polarization converters based on U-shaped graphene metamaterials," Opt. Express **27**(23), 33826–33839 (2019).
6. D. M. Pozar, "Flat lens antenna concept using aperture coupled microstrip patches," Electron. Lett. **32**(23), 2109–2111 (1996).
7. T. J. Cui, M. Q. Qi, X. Wan, J. Zhao, and Q. Cheng, "Coding metamaterials, digital metamaterials and programmable metamaterials," Light: Sci. Appl. **3**(10), e218 (2014).
8. L. Yan, W. Zhu, M. F. Karim, H. Cai, A. Y. Gu, Z. Shen, P. H. J. Chong, D. Kwong, C. Qiu, and A. Q. Liu, "$0.2\lambda_0$ thick adaptive retroreflector made of spin-locked metasurface," Adv. Mater. **30**(39), 1802721 (2018).
9. Y. Shen, C. W. Hsu, Y. X. Yeng, J. D. Joannopoulos, and M. Soljacic, "Broadband angular selectivity of light at the nanoscale: progress, applications, and outlook," Appl. Phys. Rev. **3**(1), 011103 (2016).
10. P. Franchi and R. Mailloux, "Theoretical and experimental study of metal grid angular filters for sidelobe suppression," IEEE Trans. Antennas Propag. **31**(3), 445–450 (1983).
11. Y. Lee, S. H. Jeong, W. S. Park, J. S. Yun, and S. I. Jeon, "Multi-layer spatial angular filter with air gap tuner to suppress the grating lobes of microstrip patch arrays," in *Proceedings of IEEE MTT-S International Microwave Symposium Digest* (2002), pp. 1329–1332.

Optics EXPRESS

12. J. H. Atwater, P. Spinelli, E. Kosten, J. Parsons, C. Van Lare, J. Van de Groep, J. G. De Abajo, A. Polman, and H. A. Atwater, "Microphotonic parabolic light directors fabricated by two-photon lithography," Appl. Phys. Lett. **99**(15), 151113 (2011).
13. E. D. Kosten, J. H. Atwater, J. Parsons, A. Polman, and H. A. Atwater, "Highly efficient GaAs solar cells by limiting light emission angle," Light: Sci. Appl. **2**(1), e45 (2013).
14. Y. Xie, A. R. Zakharian, J. V. Moloney, and M. Mansuripur, "Optical transmission at oblique incidence through a periodic array of sub-wavelength slits in a metallic host," Opt. Express **14**(22), 10220–10227 (2006).
15. C. Argyropoulos, G. D'Aguanno, N. Mattiucci, N. Akozbek, M. J. Bloemer, and A. Alù, "Matching and funneling light at the plasmonic Brewster angle," Phys. Rev. B **85**(2), 024304 (2012).
16. Y. Shen, D. Ye, I. Celanovic, S. G. Johnson, J. D. Joannopoulos, and M. Soljacic, "Optical broadband angular selectivity," Science **343**(6178), 1499–1501 (2014).
17. Y. Shen, D. Ye, L. Wang, I. Celanovic, L. Ran, J. D. Joannopoulos, and M. Soljacic, "Metamaterial broadband angular selectivity," Phys. Rev. B **90**(12), 125422 (2014).
18. H. Huang and Z. Shen, "Angle-selective surface based on uniaxial dielectric-magnetic slab," Antennas Wirel. Propag. Lett. **19**(12), 2457–2461 (2020).
19. J. D. Ortiz, J. D. Baena, V. Losada, F. Medina, and J. L. Araque, "Spatial angular filtering by FSSs made of chains of interconnected SRRs and CSRRs," IEEE Microw. Wireless Compon. Lett. **23**(9), 477–479 (2013).
20. V. A. Fedotov, J. Wallauer, M. Walther, M. Perino, N. Papasimakis, and N. I. Zheludev, "Wavevector selective metasurfaces and tunnel vision filters," Light: Sci. Appl. **4**(7), e306 (2015).
21. P. Rodríguez-Ulibarri and M. Beruete, "Nonbianisotropic complementary split ring resonators as angular selective metasurfaces," J. Opt. Soc. Am. **34**(7), D56 (2017).
22. J. B. Pendry, A. J. Holden, D. J. Robbins, and W. J. Stewart, "Magnetism from conductors and enhanced nonlinear phenomena," IEEE Trans. Microwave Theory Techn. **47**(11), 2075–2084 (1999).
23. F. Costa, A. Monorchio, and G. Manara, "Efficient analysis of frequency-selective surfaces by a simple equivalent-circuit model," IEEE Antennas Propag. Mag. **54**(4), 35–48 (2012).
24. F. Costa, A. Monorchio, and G. Manara, "An overview of equivalent circuit modeling techniques of frequency selective surfaces and metasurfaces," Appl. Comput. Electromagn. Soc. J. **29**(12), 960–976 (2014).
25. O. Luukkonen, C. Simovski, G. Granet, G. Goussetis, D. Lioubtchenko, A. V. Raisanen, and S. A. Tretyakov, "Simple and accurate analytical model of planar grids and high-impedance surfaces comprising metal strips or patches," IEEE Trans. Antennas Propag. **56**(6), 1624–1632 (2008).
26. A. C. D. Lima and E. A. Parker, "Fabry–Perot approach to the design of double layer FSS," IEE Proc., Microw. Antennas Propag. **143**(2), 157–162 (1996).
27. F. Medina, F. Mesa, and D. C. Skigin, "Extraordinary transmission through arrays of slits: a circuit theory model," IEEE Trans. Microwave Theory Techn. **58**(1), 105–115 (2010).